Received: 6 October 2021 | Revised: 27 November 2021 | Accepted: 2 December 2021

DOI: 10.1111/jon.12959

JOURNAL OF NEUROIMAGING
THE OFFICIAL JOURNAL OF THE AMERICAN SOCIETY OF NEUROIMAGING
WILEY

CLINICAL INVESTIGATIVE STUDY

MR diffusion and dynamic-contrast enhanced imaging to distinguish meningioma, paraganglioma, and schwannoma in the cerebellopontine angle and jugular foramen

Yoshiaki Ota[1] | Eric Liao[1] | Aristides A. Capizzano[1] | Hajime Yokota[2] | Akira Baba[1] | Ryo Kurokawa[1] | Mariko Kurokawa[1] | Toshio Moritani[1] | Kengo Yoshii[3] | Ashok Srinivasan[1]

[1] Division of Neuroradiology, Department of Radiology, University of Michigan, Ann Arbor, Michigan, USA

[2] Department of Diagnostic Radiology and Radiation Oncology, Graduate School of Medicine, Chiba University, Chiba, Japan

[3] Department of Mathematics and Statistics in Medical Sciences, Kyoto Prefectural University of Medicine, Kyoto, Japan

Correspondence
Yoshiaki Ota, Division of Neuroradiology, Department of Radiology, University of Michigan, 1500 E Medical Center Dr, UH B2, Ann Arbor, MI 48109, USA.
Email: yoshiako@med.umich.edu

Funding information: There was no funding or grant support for this study.

Abstract

Background and Purpose: Differentiation of meningiomas, paragangliomas, and schwannomas in the cerebellopontine angle and jugular foramen remains challenging when conventional MRI findings are inconclusive. This study aimed to assess the clinical utility of diffusion-weighted imaging (DWI) and dynamic contrast-enhanced MRI (DCE-MRI) findings for tumor type differentiation and to identify the most significant diagnostic parameters.

Methods: This retrospective study included 57 patients with pathologically confirmed meningiomas, paragangliomas, and schwannomas, diagnosed between January 2018 and August 2021. DWI and DCE-MRI were obtained before surgery. The apparent diffusion coefficient (ADC) and DCE-MRI parameters were calculated. The Kruskal-Wallis H test and post hoc test with Bonferroni correction and receiver operating characteristic curve were used for statistical analysis.

Results: There were 20 meningiomas (6 men; 62.3 ± 17.8 years), 23 paragangliomas (3 men; 51.6 ± 17.0 years), and 14 schwannomas (7 men; 37.7 ± 20.0 years). V_p showed a significant difference in each comparison ($p < .001$, <.001, and <.001, respectively), V_e showed significant differences both in meningiomas and paragangliomas, and paragangliomas and schwannomas ($p < .001$ and .017, respectively), and K_{trans} showed significant differences both in meningiomas and paragangliomas, and meningiomas and schwannomas ($p = .0018$ and <.001, respectively), though there was no significant difference in ADC. V_p diagnostic performance values for each pair of tumors were area under the curve of 0.89-1.00, with cutoff values of 0.14-0.27.

Conclusion: DCE-MRI can provide promising parameters to differentiate meningiomas, paragangliomas, and schwannomas in the cerebellopontine angle and jugular foramen.

KEYWORDS
DCE-MRI, DWI, meningiomas, paraganglioma, schwannomas

INTRODUCTION

The cerebellopontine angle cistern and jugular foramen are two regions commonly involved in tumors, such as meningiomas, schwannomas, and paragangliomas.[1,2] These tumors can demonstrate typical findings on conventional imaging. On CT and MRI scans, meningiomas can present as homogeneously enhancing tumors with an associated dural tail, calcification, or skull base hyperostosis.[3,4] Schwannomas can present as heterogeneously enhancing tumors with cystic changes,[5,6] and paragangliomas can present as heterogeneously enhancing tumors with prominent flow voids, necrotic or cystic changes, and a "salt and pepper" signal pattern.[7,8] These typical findings can help to differentiate among these tumor types; however, such differentiation is challenging when these imaging characteristics are not present or overlap. Accurate diagnosis is required for effective surveillance and treatment strategies. Definite diagnosis is usually obtained by histological investigation. However, biopsy is invasive and carries risks associated with the proximity of multiple nerves and vascular structures, specifically, in the jugular foramen. Therefore, imaging findings play an important role in differential diagnosis.

Diffusion-weighted imaging (DWI) and dynamic contrast-enhanced MRI (DCE-MRI) can help to differentiate tumors based on their unique microstructure, vascularity, and permeability patterns. The apparent diffusion coefficient (ADC) map is calculated from DWI findings with different *b*-values, which are usually $b = 0$ and 1000 s/mm^2; the calculated ADC values have been shown to assist in both differentiation of head and neck tumors, and evaluation of treatment effects in the head and neck.[9–11] The quantitative parameters of DCE-MRI are based on the extended Tofts model, which allows pixel-based parameter maps to be calculated from time intensity curves. The calculated parameters include fractional plasma volume (V_p), fractional volume of extracellular space per unit volume of tissue (V_e), and forward volume transfer constant (K_{trans}). V_p is thought to reflect tumor vascularity, while V_e and K_{trans} represent permeability.[12,13] Meningiomas, schwannomas, and paragangliomas have different internal histoarchitecture, blood flow, and vascular permeability, which suggests that DWI and DCE-MRI can help to differentiate among them. Previous studies have explored the differentiation of head and neck schwannomas and paragangliomas using DWI and DCE-MRI scans; one study has shown that V_p may be the most significant parameter in differentiating these lesions.[14] However, the utility of DWI and DCE-MRI scans for differentiating intracranial meningiomas from schwannomas and paragangliomas has not been fully investigated.

In this study, we aimed to examine the role of DWI and DCE-MRI findings in differentiating the most common tumors in the cerebellopontine angle and jugular foramen, including meningiomas, paragangliomas, and schwannomas.

METHODS

Our institutional review board approved this retrospective single-center study and waived the requirement for informed consent. Data were acquired in compliance with all applicable Health Insurance Portability and Accountability Act regulations.

Study population

We retrospectively reviewed 843 patients suspected of tumors in the cerebellopontine angle or jugular foramen at our institution between January 2018 and August 2021. Among 843 patients, 85 had pathologically confirmed tumors in the cerebellopontine angle and jugular foramen, including 35 meningiomas, 30 paragangliomas, and 20 schwannomas. We excluded patients who did not have pretreatment DWI or DCE-MRI data, or had been treated with surgery, radiotherapy, or embolization prior to DWI and DCE-MRI sequence acquisition. In total, 57 patients (16 men; mean age, 51.2 ± 17.8 years) with 20 meningiomas, 23 paragangliomas, and 14 schwannomas were included in this study.

Image acquisition

All MRI examinations were performed using 1.5 T and 3 T scanners (Philips, Ingenia, Eindhoven) and using a 16-channel neurovascular coil. Acquired sequences included axial T2-weighted image (T2WI), T1-weighted image (T1WI), axial and coronal pre and postcontrast-enhanced fat-sat T1WI, and DWI scans using echo-planar imaging with the following parameters: repetition time (TR) range: 5000-10,000 milliseconds; echo time (TE) range: 58-106 milliseconds; number of excitation (NEX): 1-2; slice thickness/gap: 4/0-1 mm; field of view: 240 mm × 240 mm; pixel size: 1.5 × 1.5 mm; and three diffusion directions. Sensitizing diffusion gradients were applied sequentially with *b*-values of 0 and 1000 s/mm^2.

DCE-MRI scanning was performed using a 3-dimensional T1-weighted fast field echo (FFE). The parameters of 3D-T1 FFE were as follows: TR = 4.6 milliseconds; TE = 1.86 milliseconds; flip angles = 5°, 10°, 15°, 20°, and 30°; slice thickness = 2.5 mm; field of view = 240 × 240 mm^2; voxel size = 1.0×1.0×5.0 mm^3; NEX = 1; number of slices per dynamic scan = 48; temporal resolution = 8.4 seconds; and total acquisition time of 4 minutes and 13 seconds. An intravenous bolus of 20 ml gadobenate dimeglumine contrast (Multihance, Bracco Diagnostics, Singen, Germany) was administered using a power injector with a flow rate of 5.0 ml/s through a peripheral arm vein, followed by a 20 ml saline flush.

Conventional imaging, ADC, and DCE-MRI analysis

Two board-certified radiologists with 7 (Y.O.) and 13 (A.B.) years of experience independently evaluated conventional imaging findings and performed ADC and DCE-MRI analysis. The histopathological results were blinded to the two readers.

The following conventional imaging features were evaluated:

1. Cystic changes, defined as nonenhancing, predominantly T2 hyperintense areas.
2. Necrotic changes, defined as nonenhancing, predominantly T1 hypointense, and heterogeneously T2 hyperintense areas.

The maximum axial diameter was measured using postcontrast-enhanced fat-sat T1WI imaging by a radiologist with 7 years of experience (Y.O.).

ADC maps were constructed with a monoexponential fitting model using commercially available software (OleaSphere, Version 3.0; Olea Medical, La Ciotat, France). The same two board-certified neuroradiologists independently contoured the freehand region of interest (ROI) on the ADC map in reference to axial postcontrast-enhanced T1WI findings. A single ROI was placed on each tumor. Both neuroradiologists adhered to the following procedure:

1. ROIs were placed where the tumors predominantly showed solid-enhancing portions without cystic or necrotic areas.
2. Peripheral 2-mm margins of the lesions were spared to avoid volume averaging.
3. ROI location and size were adjusted when geometric distortion was observed on the ADC map.

As an internal standard, an ROI was placed within the cervical spinal cord at the level of the C1-C2 disc space, which was included in the field of view of every study. A normalized ADC ratio ($nADC_{mean}$) was calculated by dividing each lesion ADC value by the spinal cord ADC value to adjust for the variation of ADC values across MRI scanners, magnetic field strengths, and matrix sizes.

All quantitative analyses of DCE-MRI data were performed using the OleaSphere 3.0 software permeability module, which is based on the extended Tofts model, by which pixel-based parameter maps were calculated from time intensity curves. The two radiologists independently placed a freehand ROI on the permeability maps and included the enhancing components of the tumors without cystic or necrotic areas, while sparing the peripheral 2 mm of lesions. The calculated quantitative parameters were V_p, V_e, K_{trans}, and K_{ep}. The arterial input function was automatically computed, and the corresponding curves with a rapid increase in signal enhancement and sharp peaks were chosen for DCE analysis.

Statistical analysisroc

The $nADC_{mean}$, calculated from ADC analysis, and V_p, V_e, and K_{trans}, calculated from DCE-MRI analysis, were compared between the three tumor types using the Kruskal-Wallis H test and post hoc test with Bonferroni correction. For comparison of each of the two tumor types (meningiomas vs. paragangliomas, meningiomas vs. schwannomas, and paragangliomas vs. schwannomas), $nADC_{mean}$, V_p, V_e, and K_{trans} were compared by Mann-Whitney U test with Bonferroni correction. Statistically significant diagnostic differentiators in Mann-Whitney U test were used forreceiver operating characteristic (ROC) curve analysis. The optimal cutoff values in the ROC curve analysis were determined to maximize the Youden index (sensitivity + specificity – 1).

Inter-reader agreement for conventional imaging features was assessed using the kappa coefficient, and for quantitative parameters of the mean ADC, normalized mean ADC, V_e, and V_p values, it was assessed using the intraclass correlation coefficient. All statistical calculations were conducted using R software (version 4.1.1; R Core Team, Vienna, Austria). Variables with p-values of $< .05$ were considered statistically significant.

RESULTS

This study included 20 cases of meningiomas (6 men; mean age, 62.3 ± 17.8 years), including 16 and 4 World Health Organization (WHO) grade I and II meningiomas, respectively; 23 cases of paragangliomas (3 men; mean age, 51.6 ± 17.0 years); and 14 cases of schwannomas (7 men; mean age, 37.7 ± 20.0 years). Patient demographic characteristics and conventional imaging findings are summarized in Table 1.

DWI and DCE variables

The Kruskal-Wallis H test and post hoc test with Bonferroni correction showed that there were statistically significant differences in all quantitative DCE-parameters among meningioma, paraganglioma, and schwannoma ($p < .001$), while there was no significant difference in $nADC_{mean}$. The comparisons of ADC and quantitative DCE-MRI parameters among the three tumors are summarized in Table 2 and Figure 1.

In Mann-Whitney U test with Bonferroni correction for ADC analysis, there was no significant difference in $nADC_{mean}$ between meningiomas versus paragangliomas (median 1.36 [1.23-1.52] vs. 1.38 [1.33-1.55]; $p > .99$), meningiomas versus schwannomas (median 1.36 [1.23-1.52] vs. 1.41 [1.38-1.54]; $p > .99$), or paragangliomas versus schwannomas (median 1.38 [1.33-1.55] vs. 1.41 [1.38-1.54]; $p > .99$).

In Mann-Whitney U test with Bonferroni correction for DCE-MRI analysis, V_e, V_p, and K_{trans} were significantly different between meningiomas versus paragangliomas (V_e: median 0.50 [0.33-0.64] vs. 0.17 [0.078-0.27]; $p = .002$, V_p: median 0.20 [0.18-0.22] vs. 0.47 [0.39-0.59]; $p < .001$, and K_{trans} (minute^{-1}): median 0.72 [0.45-1.04] vs. 0.08 [0.025-0.23]; $p = .007$, respectively). Between meningioma versus schwannomas, V_p and K_{trans} values were significantly different (V_p: median 0.200 [0.18-0.22] vs. 0.065 [0.043-0.095]; $p = .002$, K_{trans} (minute^{-1}): median 0.72 [0.45-1.04] vs. 0.17 [0.11-0.27]; $p = .002$, respectively), while there was no difference in V_e between meningiomas versus schwannomas (V_e: median 0.50 [0.33-0.64] vs. 0.44 [0.33-0.53]; $p > .99$). Between paragangliomas versus schwannomas, V_p was significantly different (V_p: median 0.47 [0.39-0.59] vs. 0.065 [0.043-0.095]; $p < .001$, respectively), while V_e and K_{trans} were not significantly different (V_e: median 0.17 [0.078-0.27] vs. 0.44 [0.33-0.53]; $p = .07$, K_{trans} [minute^{-1}]: median 0.08 [0.025-0.23] vs. 0.17 [0.11-0.27]; $p > .99$, respectively).

TABLE 1 Patient demographic and conventional imaging characteristics

	Meningioma	Paraganglioma	Schwannoma
Numbers of the patients	20	23	14
Sex (male/female)	6/14	3/20	7/7
Age (years)	62.3 ± 17.8	51.6 ± 17.0	37.7 ± 20.0
Maximum axial diameter (mm)	19.5 (11-34)	28.7 (15-60)	30.9 (14-40)
Main location (CPA/jugular foramen)	12/8	0/23	6/8
Presence of cystic/necrotic change	2/20	14/23	8/14

Note: Values presented as the mean ± standard deviation or median (range).
Abbreviation: CPA, cerebellopontine angle.

TABLE 2 DWI and DCE-MRI parameters of meningiomas, paragangliomas, and schwannomas and Kruskal-Wallis H test and post hoc test with Bonferroni correction

					p Value[b]		
	Meningiomas	Paragangliomas	Schwannomas	*p* Value[a]	Meningiomas versus paragangliomas	Meningiomas versus schwannomas	Paragangliomas versus schwannomas
$nADC_{mean}$	1.36 [1.23-1.52]	1.38 [1.33-1.55]	1.41 [1.38-1.54]	.48	$p = 1.0$	$p = .88$	$p = 1.0$
V_p	0.20 [0.18-0.22]	0.47 [0.39-0.59]	0.065 [0.043-0.095]	<.001	$p < .001$	$p < .001$	$p < .001$
V_e	0.50 [0.33-0.64]	0.17 [0.078-0.27]	0.44 [0.33-0.53]	<.001	$p < .001$	$p = 1.0$	$p = .017$
K_{trans} ($minute^{-1}$)	0.72 [0.45-1.04]	0.08 [0.025-0.23]	0.17 [0.11-0.27]	<.001	$p = .0018$	$p < .001$	$p = .42$

Note: Data presented as median with interquartile ranges in parentheses.
Abbreviations: ADC_{mean}, normalized mean apparent diffusion coefficient; K_{trans}, forward volume transfer constant; V_e, extravascular extracellular space; V_p, fractional plasma volume.
[a]*p* Value is from Kruskal-Wallis H test.
[b]*p* Value is adjusted for pairwise comparison by Bonferroni correction.

Table 3 and Figure 2 demonstrate the diagnostic performance of DCE-MRI parameters, which showed significant differences between meningiomas versus paragangliomas, meningiomas versus schwannomas, and paragangliomas versus schwannomas. Representative cases of meningiomas, paragangliomas, and schwannomas with ADC and DCE-MRI analysis are shown in Figures 3-5.

Inter-reader agreement for conventional imaging features and quantitative parameters was excellent (Table 4).

DISCUSSION

This study aimed to assess the clinical utility of DWI and DCE-MRI findings for differentiating meningiomas, paragangliomas, and schwannomas in the cerebellopontine angle and jugular foramen. V_p helped to distinguish all three tumor types, whereas V_e was useful in distinguishing paragangliomas from meningiomas and schwannomas, and K_{trans} in distinguishing meningiomas from paragangliomas and schwannomas by Kruskal-Wallis H test. ROC analysis revealed that the diagnostic performance of V_p was 0.89-1.00 AUCs with the cutoffs of 0.14-0.27 in the three tumors; meanwhile, the diagnostic performance of K_{trans} in meningiomas versus paragangliomas and meningiomas versus schwannomas was 0.81-0.89 AUCs with the cutoffs of 0.26-0.36, and the performance of V_e in meningiomas versus paragangliomas was 0.85 AUC with the cutoff of 0.22. Normalized mean ADC values did not show any difference between the tumor types.

There were 16 and 4 WHO grade I and II meningiomas, respectively; however, previous studies have shown similarities in ADC values between grade I and II meningiomas.[15–17] These findings suggest that combining grade I and II meningiomas may not impact the mean ADC values when evaluating meningiomas as a cohort.

A previous study in paragangliomas has shown that a succinate dehydrogenase gene mutation can lower ADC values due to differences in flow voids, cellularity, or other internal structures.[18] Consistent with the present findings, a separate previous study failed to show any significant difference in ADC values between paragangliomas and schwannomas in the head and neck regions.[14] This finding may reflect the internal structures of the two tumor types, which may overlap due to heterogeneous succinate dehydrogenase mutation status of paragangliomas and/or differences in the internal structures of schwannomas, which show a biphasic pattern of high cellularity (Antoni A) and fewer cells with cystic or xanthomatous changes (Antoni B).

ADC values of schwannomas can vary, as reported in prior studies, which may be because schwannomas show different histological

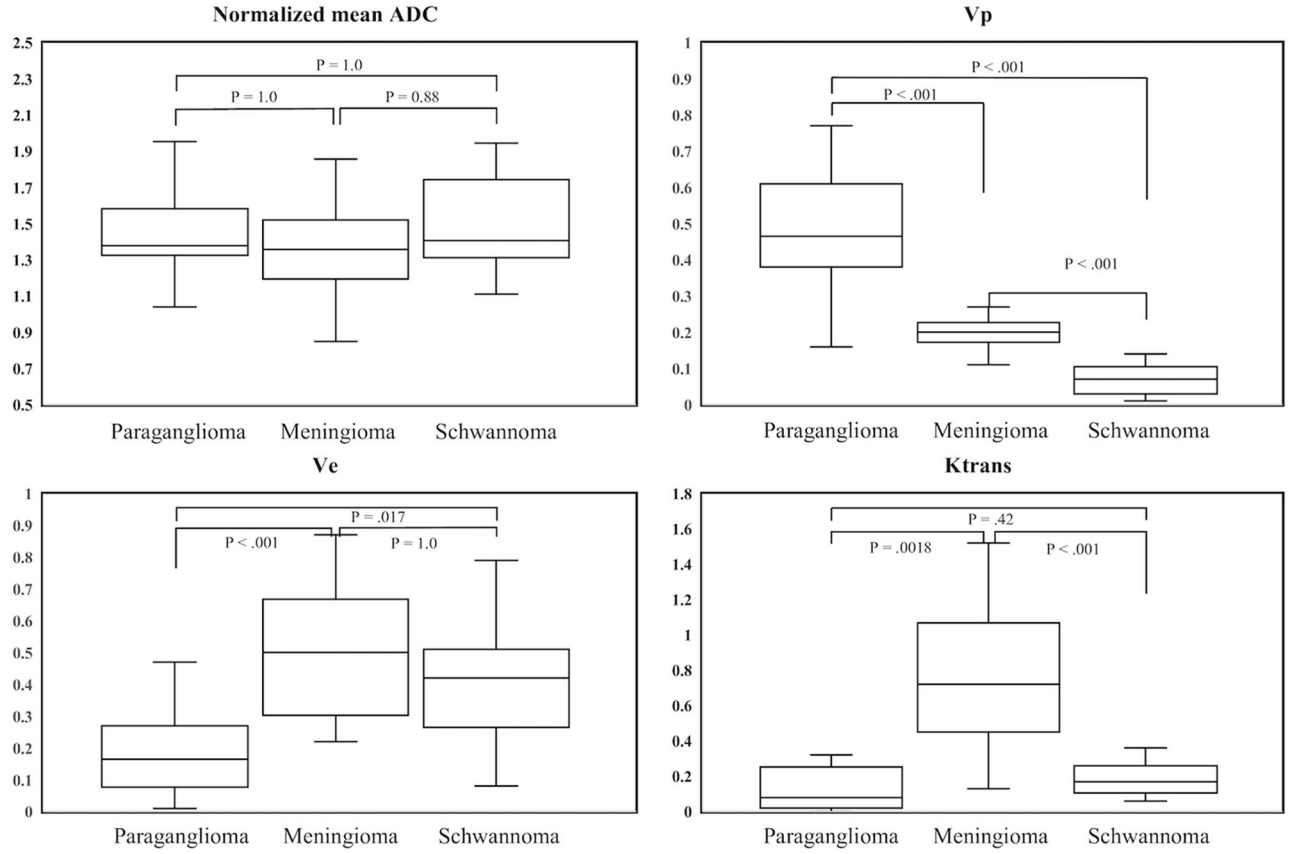

FIGURE 1 Box-and-whisker plots show DWI and DCE-MRI parameters for all cases with Kruskal-Wallis H test and post hoc test with Bonferroni correction. Boundaries of boxes indicate 25th and 75th percentiles, and lines in boxes indicate medians

TABLE 3 Diagnostic performance of DCE-MRI parameters

	Meningioma versus paraganglioma			Meningioma versus schwannoma		Paraganglioma versus schwannoma
Parameters	V_p	V_e	K_{trans} (minute^{-1})	V_p	K_{trans} (minute^{-1})	V_p
Cutoff	0.27	0.22	0.26	0.14	0.36	0.14
Sensitivity	0.91	1.00	0.90	0.93	0.93	0.93
Specificity	0.90	0.68	0.77	0.80	0.80	1.00
PPV	0.91	0.74	0.78	0.77	0.77	1.00
NPV	0.90	1.00	0.90	0.94	0.94	0.96
Accuracy	0.91	0.83	0.83	0.85	0.85	0.97
AUC	0.94	0.85	0.81	0.89	0.89	1.00

Abbreviations: AUC, area under the curve; K_{trans}, forward volume transfer constant; NPV, negative predictive value; PPV, positive predictive value; V_e, extravascular extracellular space; V_p, fractional plasma volume.

compositions, such as Antoni A and Antoni B tissue patterns, which are not evident on conventional MRI sequences. Some studies have shown that schwannomas have higher ADC values than meningiomas.[5,17,19] However, other studies have shown that larger schwannomas are more likely to undergo cystic changes,[20] which might result in high ADC values. The similarities in ADC values between schwannomas and paragangliomas might be due to the exclusion of cystic/necrotic changes from ROIs and the size of schwannomas, which were relatively small in the studied anatomical locations.

DCE-MRI can help to assess tumor microvasculature and permeability. This technique has been used for both characterization and differentiation of tumors and prediction of treatment effect in the

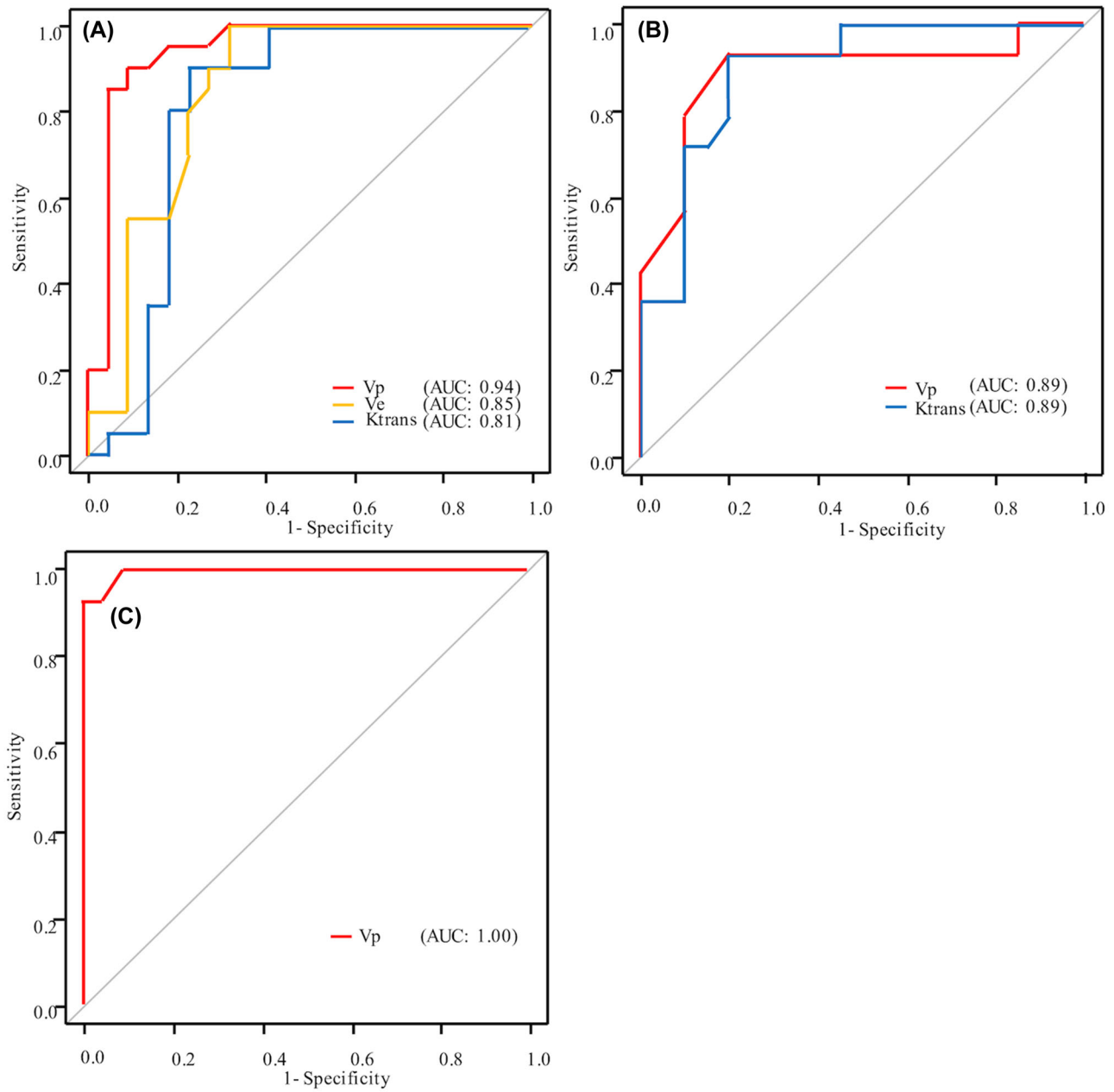

FIGURE 2 Receiver operating characteristic curves of (A) meningioma versus paraganglioma, (B) meningioma versus schwannoma, and (C) paraganglioma versus schwannoma. Abbreviation: AUC, area under the curve

head and neck.[12,21–23] ROIs were placed within the enhancing component of the tumors, avoiding the portions that mainly showed cystic/necrotic components, which could have lower the values of DCE-MRI parameters.

V_p values represent tumor microvasculature, and V_e and K_{trans} values reflect tumor permeability.[13,14,23,24] In the present study, K_{trans}, V_e, and V_p values were statistically different between meningiomas and paragangliomas, and K_{trans} and V_p were statistically different between paragangliomas and schwannomas; meanwhile, only V_p helped differentiate between meningiomas and schwannomas by Mann-Whitney U test with Bonferroni correction. Higher K_{trans} and V_e and lower V_p values in meningiomas may reflect higher permeability and lower microvasculature density in this tumor type than those observed in paragangliomas. In addition, V_p and K_{trans} values were higher in meningiomas than in schwannomas, and could represent higher microvasculature density and permeability in the former than in the latter tumor type. Higher V_p values in paragangliomas may reflect higher vascularity in this tumor type than that observed in schwannomas, as previously reported in a study of nonbiopsy-confirmed paragangliomas and schwannomas.[25]

Among the DCE-MRI parameters in our study, V_p was significantly different in the three tumors, both by the Kruskal-Wallis H test and Mann-Whitney U test, and with promising diagnostic performances in ROC analysis, suggesting that the difference in microvasculature

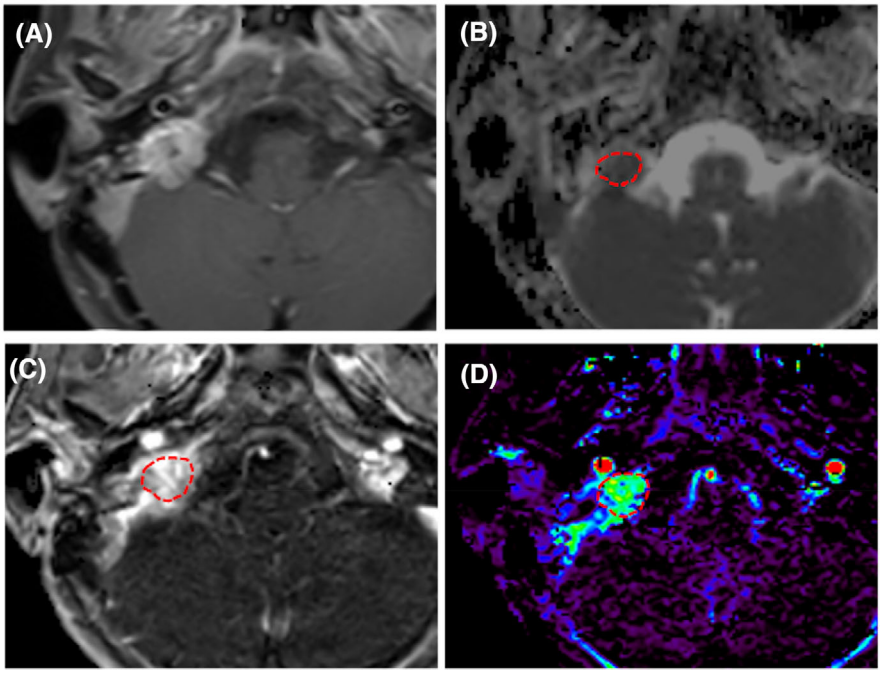

FIGURE 3 Images of a 57-year-old woman with meningioma in the right jugular foramen. (A) Axial contrast-enhanced T1-weighted with fat saturation image shows a heterogeneously enhancing mass in the right jugular foramen. (B) A freehand region of interest (dotted line) was placed on the apparent diffusion coefficient (ADC) map, and the mean and normalized ADC values were 1.12×10^{-3} mm^2/s and 1.4, respectively. (C) A freehand region of interest was placed on the permeability map, and DCE-MRI parameters were calculated. (D) V_p reveals 0.19

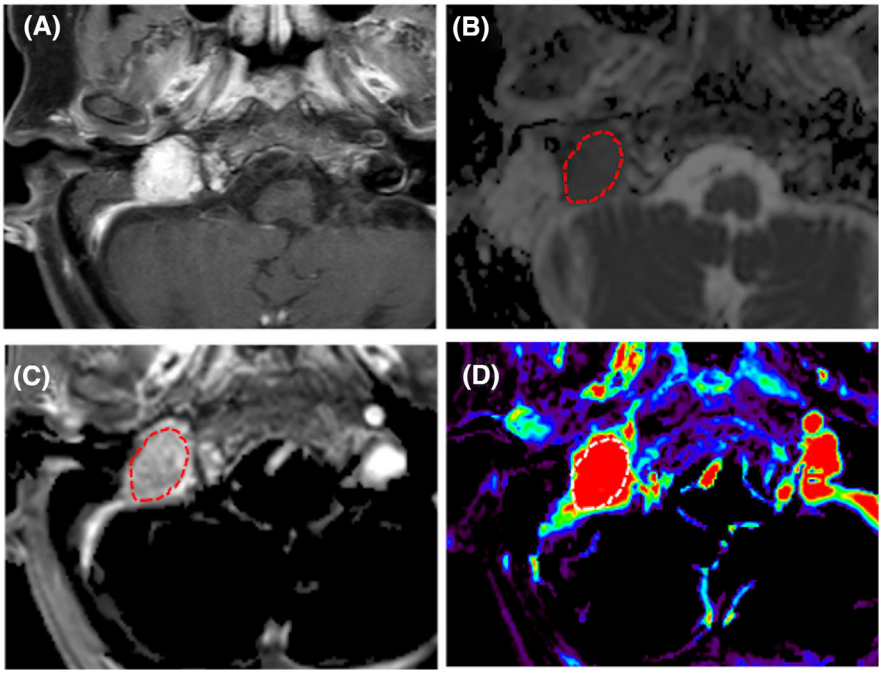

FIGURE 4 Images of a 76-year-old woman with paraganglioma in the right jugular foramen. (A) Axial contrast-enhanced T1-weighted image with fat saturation shows a heterogeneously enhancing mass in the right jugular foramen. (B) A freehand region of interest was placed on the apparent diffusion coefficient (ADC) map, and the mean and normalized ADC values were 1.07×10^{-3} mm^2/s and 1.43, respectively. (C) A freehand region of interest was placed on the permeability map, and DCE-MRI parameters were calculated. (D) V_p reveals 0.39

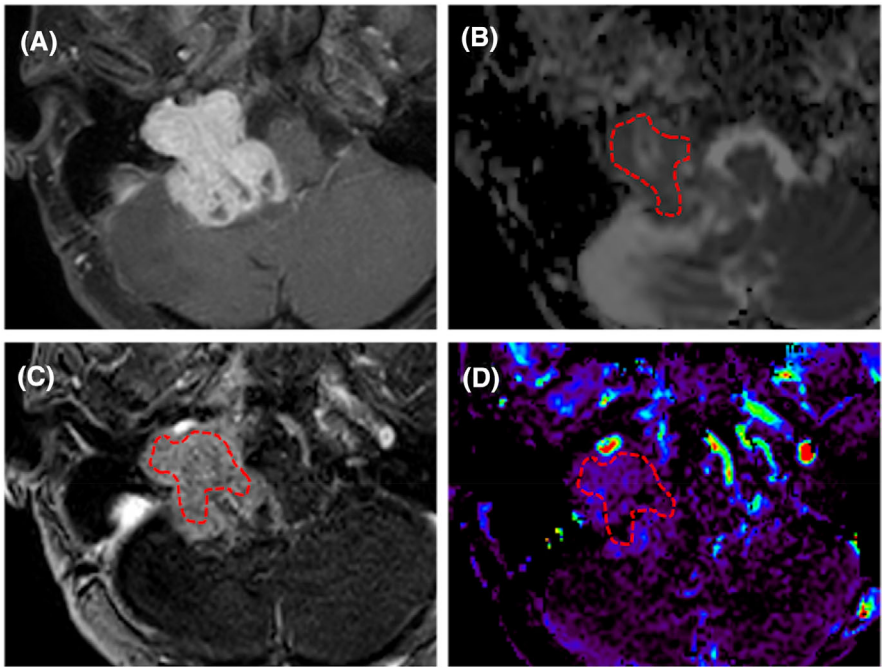

FIGURE 5 Images of a 36-year-old man with schwannoma in the right jugular foramen. (A) Axial contrast-enhanced T1-weighted image with fat saturation shows a heterogeneously enhancing mass with cystic changes in the right jugular foramen. (B) A freehand region of interest was placed on the apparent diffusion coefficient (ADC) map, avoiding the cystic component, which was defined as nonenhanced, predominantly in the T2 hyperintense area. The mean and normalized ADC values were 0.90×10^{-3} mm^2/s and 1.2, respectively. (C) A freehand region of interest was placed on the permeability map, and DCE-MRI parameters were calculated. (D) V_p reveals 0.06

TABLE 4 Inter-reader agreement for conventional imaging features and quantitative parameters

Metrics	Reader 1 versus reader 2
Cystic/necrotic change	0.950
Normalized mean ADC	0.900
V_e	0.878
V_p	0.858
K_{trans} (minute^{-1})	0.885

Note: Agreement was assessed for conventional imaging findings by Cohen's kappa and for quantitative parameters by intraclass correlation coefficient. Abbreviations: ADC, apparent diffusion coefficient; K_{trans}, forward volume transfer constant; V_e, extravascular extracellular space; V_p, fractional plasma volume.

among the three tumor types may help improve diagnostic accuracy. The present findings suggest the benefits of using DCE-MRI scanning in head and neck MRI protocols, specifically, when conventional imaging does not reveal typical imaging features, or the imaging features overlap.

This study had several limitations. First, this was a retrospective, single-center study with a small sample size. However, we were able to identify a single most significant tumor type differentiator based on DCE-MRI parameters. Second, we used 1.5 T and 3 T scanners for this study.[26] DCE-MRI parameters can vary based on vendors, scanners, and magnetic field strengths.[26] The difference in magnetic field strengths may add heterogeneity to the calculated parameters. For ADC analysis, the cervical cord at the C1-C2 level was selected to normalize the ADC values. The cervical cord is less commonly affected by chronic microvascular disease or direct tumor invasion, and this level is usually included in head and neck imaging protocols. Finally, even though the scan readers were blinded to the histological findings, any pre-existing knowledge of tumor morphologic features may have affected the placing of ROIs for ADC and DCE-MRI analyses.

In conclusion, DCE-MRI parameters can help in the differentiation of meningiomas, paragangliomas, and schwannomas, which are the most common primary masses in the cerebellopontine angle and jugular space. In contrast, DWI is unlikely to support the differentiation of these lesions. When differential diagnosis is challenging, adding DCE-MRI scanning to the head and neck protocol may be warranted.

ACKNOWLEDGMENTS AND DISCLOSURE

The authors declare no conflicts of interest.

ORCID

Yoshiaki Ota https://orcid.org/0000-0001-8992-2156
Akira Baba https://orcid.org/0000-0001-6913-5307
Mariko Kurokawa https://orcid.org/0000-0002-3907-9188

REFERENCES

1. Vogl TJ, Bisdas S. Differential diagnosis of jugular foramen lesions. Skull Base 2009;19:3-16.

2. Smirniotopoulos JG, Yue NC, Rushing EJ. Cerebellopontine angle masses: radiologic-pathologic correlation. Radiographics 1993;13:1131-47.
3. Tokgoz N, Oner YA, Kaymaz M, Ucar M, Yilmaz G, Tali ET. Primary intraosseous meningioma: CT and MRI appearance. AJNR Am J Neuroradiol 2005;26:2053-6.
4. Macdonald AJ, Salzman KL, Harnsberger HR, Gilbert E, Shelton C. Primary jugular foramen meningioma: imaging appearance and differentiating features. AJR Am J Roentgenol 2004;182:373-7.
5. Skolnik AD, Loevner LA, Sampathu DM, et al. Cranial nerve schwannomas: diagnostic imaging approach. Radiographics 2016;36:1463-77.
6. Mulkens TH, Parizel PM, Martin JJ, et al. Acoustic schwannoma: MR findings in 84 tumors. AJR Am J Roentgenol 1993;160:395-8.
7. Olsen WL, Dillon WP, Kelly WM, Norman D, Brant-Zawadzki M, Newton TH. MR imaging of paragangliomas. AJR Am J Roentgenol 1987;148:201-4.
8. Williams MD. Paragangliomas of the head and neck: an overview from diagnosis to genetics. Head Neck Pathol 2017;11:278-87.
9. Surov A, Meyer HJ, Wienke A. Apparent diffusion coefficient for distinguishing between malignant and benign lesions in the head and neck region: a systematic review and meta-analysis. Front Oncol 2020;9:1362.
10. Kanmaz L, Karavas E. The role of diffusion-weighted magnetic resonance imaging in the differentiation of head and neck masses. J Clin Med 2018;7:130.
11. Hoang JK, Choudhury KR, Chang J, Craciunescu OI, Yoo DS, Brizel DM. Diffusion-weighted imaging for head and neck squamous cell carcinoma: quantifying repeatability to understand early treatment-induced change. AJR Am J Roentgenol 2014;203:1104-8.
12. Gaddikeri S, Gaddikeri RS, Tailor T, Anzai Y. Dynamic contrast-enhanced MR imaging in head and neck cancer: techniques and clinical applications. AJNR Am J Neuroradiol 2016;37:588-95.
13. Jung SC, Yeom JA, Kim JH, et al. Glioma: application of histogram analysis of pharmacokinetic parameters from T1-weighted dynamic contrast-enhanced MR imaging to tumor grading. AJNR Am J Neuroradiol 2014;35:1103-10.
14. Ota Y, Liao E, Capizzano AA, et al. Diagnostic role of diffusion-weighted and dynamic contrast-enhanced perfusion MR imaging in paragangliomas and schwannomas in the head and neck. AJNR Am J Neuroradiol 2021;42:1839-46.
15. Yamasaki F, Kurisu K, Satoh K, et al. Apparent diffusion coefficient of human brain tumors at MR imaging. Radiology 2005;235:985-91.
16. Sanverdi SE, Ozgen B, Oguz KK, et al. Is diffusion-weighted imaging useful in grading and differentiating histopathological subtypes of meningiomas? Eur J Radiol 2012;81:2389-95.
17. Pavlisa G, Rados M, Pazanin L, Padovan RS, Ozretic D, Pavlisa G. Characteristics of typical and atypical meningiomas on ADC maps with respect to schwannomas. Clin Imaging 2008;32:22-7.
18. Ota Y, Naganawa S, Kurokawa R, et al. Assessment of MR imaging and CT in differentiating hereditary and nonhereditary paragangliomas. AJNR Am J Neuroradiol 2021;42:1320-6.
19. Xu XQ, Li Y, Hong XN, et al. Radiological indeterminate vestibular schwannoma and meningioma in cerebellopontine angle area: differentiating using whole-tumor histogram analysis of apparent diffusion coefficient. Int J Neurosci 2017;127:183-90.
20. Mehrotra N, Behari S, Pal L, et al. Giant vestibular schwannomas: focusing on the differences between the solid and the cystic variants. Br J Neurosurg 2008;22:550-6.
21. Ota Y, Liao E, Kurokawa R, et al. Diffusion-weighted and dynamic contrast-enhanced MRI to assess radiation therapy response for head and neck paragangliomas. J Neuroimaging 2021;31:1035-43.
22. Gaddikeri S, Hippe DS, Anzai Y. Dynamic contrast-enhanced MRI in the evaluation of carotid space paraganglioma versus schwannoma. J Neuroimaging 2016;26:618-25.
23. Chidambaram S, Pannullo SC, Roytman M, et al. Dynamic contrast-enhanced magnetic resonance imaging perfusion characteristics in meningiomas treated with resection and adjuvant radiosurgery. Neurosurg Focus 2019;46:E10.
24. Jain R. Measurements of tumor vascular leakiness using DCE in brain tumors: clinical applications. NMR Biomed 2013;26:1042-9.
25. Pires A, Nayak G, Zan E, et al. Differentiation of jugular foramen paragangliomas versus schwannomas using golden-angle radial sparse parallel dynamic contrast-enhanced MRI. AJNR Am J Neuroradiol. 2021;42:1847-52.
26. Shukla-Dave A, Obuchowski NA, Chenevert TL, et al. Quantitative imaging biomarkers alliance (QIBA) recommendations for improved precision of DWI and DCE-MRI derived biomarkers in multicenter oncology trials. J Magn Reson Imaging 2019;49:e101-e21.

How to cite this article: Ota Y, Liao E, Capizzano AA, et al. MR diffusion and dynamic-contrast enhanced imaging to distinguish meningioma, paraganglioma, and schwannoma in the cerebellopontine angle and jugular foramen. J Neuroimaging. 2022;32:502–510.
https://doi.org/10.1111/jon.12959